ChemComm

COMMUNICATION

View Article Online
View Journal | View Issue

Cite this: *Chem. Commun.*, 2018, **54**, 8972

Received 5th June 2018,
Accepted 28th June 2018

DOI: 10.1039/c8cc04437f

rsc.li/chemcomm

Rapid access to RNA resonances by proton-detected solid-state NMR at >100 kHz MAS†

Alexander Marchanka,‡[a] Jan Stanek,‡[b] Guido Pintacuda[b] and Teresa Carlomagno*[ac]

Fast (>100 kHz) magic angle spinning solid-state NMR allows combining high-sensitive proton detection with the absence of an intrinsic molecular weight limit. Using this technique we observe for the first time narrow ^{1}H RNA resonances and assign nucleotide spin systems with only 200 μg of uniformly ^{13}C,^{15}N-labelled RNA.

The discovery of the three-dimensional structure of ribonucleic acids (RNA), either in isolation or in complex with proteins, is essential to explain their numerous functions in cells. The structure of RNA is best studied by Nuclear Magnetic Resonance (NMR) spectroscopy, which can cope with the inherent flexibility of the polymer. However, unlike proteins, RNA consists of building blocks of low chemical diversity, resulting in poor chemical shifts dispersion. Consequently, NMR analysis of RNAs >40–50 nucleotides requires laborious selective isotopic labeling. Furthermore, the sensitivity and the resolution of solution NMR decrease with the molecular mass, posing a practical limit of about 60–80 nucleotides.

Magic-angle spinning (MAS) solid-state NMR spectroscopy[1] does not have an intrinsic molecular weight limit and holds the potential of being applicable to RNAs of any size. Recently, MAS NMR was employed for the first time to determine *de novo* the structure of a RNA in a non-diffracting solid preparation, the 26mer Box C/D RNA in complex with the protein L7Ae from *Pyrococcus furiosus* (*Pf*).[2,3] The strategy comprised of ^{13}C- and ^{15}N-detected experiments for both resonance assignment and measurement of structural restraints. The low sensitivity of ^{13}C,^{15}N nuclei rendered high-dimensional NMR methods impractical, even when using >6–8 mg of RNA.[2,3] The severe overlap of the resonances in two-dimensional spectra was lifted using single (A, U, C, G) nucleotide-type selective labeling for the assignment of nucleotide spin systems, and double (AU, CG, *etc.*) nucleotide-type selective labeling for sequential assignment and collection of structural restraints. Despite successful, this strategy necessitated the measurement of several samples, resulting in a substantial commitment of laboratory and instrument times. ^{1}H-detection provides the highest sensitivity; nonetheless, it has long been a unique mark of solution NMR spectroscopy, because of the extreme line broadening caused in solids by the dense network of strong ^{1}H–^{1}H dipolar couplings. ^{1}H-detection at moderate (24 kHz) MAS rates was shown to be practical with perdeuteration and partial reintroduction of exchangeable protons.[4–6] However, in RNA this labeling scheme limits the NMR active probes to labile imino and amino ^{1}Hs, and prevents efficient resonance assignment strategies.[5,7,8] Faster MAS rates are necessary to lift the requirement of proton dilution and at the same time ensure sensitivity and resolution. Recently, ^{1}H detection was used on a uniformly labeled 23mer DIS HIV-1 RNA to observe base pairs through ^{15}N–^{15}N proton assisted recoupling (PAR); however, at the MAS rate of 40 kHz, the proton resolution (500 Hz) was insufficient to enable site-specific assignments.[9]

The availability of hardware that is capable to reach fast (60–100 kHz) spinning rates has been critical for the development of ^{1}H-detected MAS NMR experiments for proteins, allowing faster backbone and side-chain assignments, as well as structural and dynamics studies.[10–12] Despite its lower proton density when compared to proteins, RNA is a challenge for effective averaging of dipolar interactions by MAS, due to the spatial clustering of protons and the intrinsic flexibility. Here we show that MAS rates exceeding 100 kHz open an avenue for the study of fully protonated RNA at high resolution and sensitivity. 2D ^{1}H-detected fingerprint spectra can be acquired in minutes to hours using as little as 200 μg of RNA. This enables the exploitation of high-dimensional NMR techniques, which allow

[a] *Centre for Biomolecular Drug Research (BMWZ) and Institute of Organic Chemistry, Leibniz University Hannover, Schneiderberg 38, 30167 Hannover, Germany. E-mail: teresa.carlomagno@oci.uni-hannover.de*
[b] *Institut des Sciences Analytiques (UMR 5280 – CNRS, ENS Lyon, UCB Lyon 1), Université de Lyon, 5 rue de la Doua, 69100 Villeurbanne, France*
[c] *Helmholtz Centre for Infection Research, Group of Structural Chemistry, Inhoffenstraße 7, 38124, Braunschweig, Germany*

† Electronic supplementary information (ESI) available: Details on sample preparation, NMR spectroscopy; RF pulse sequence schemes; list of chemical shifts. See DOI: 10.1039/c8cc04437f

‡ A. M. and J. S. contributed equally.

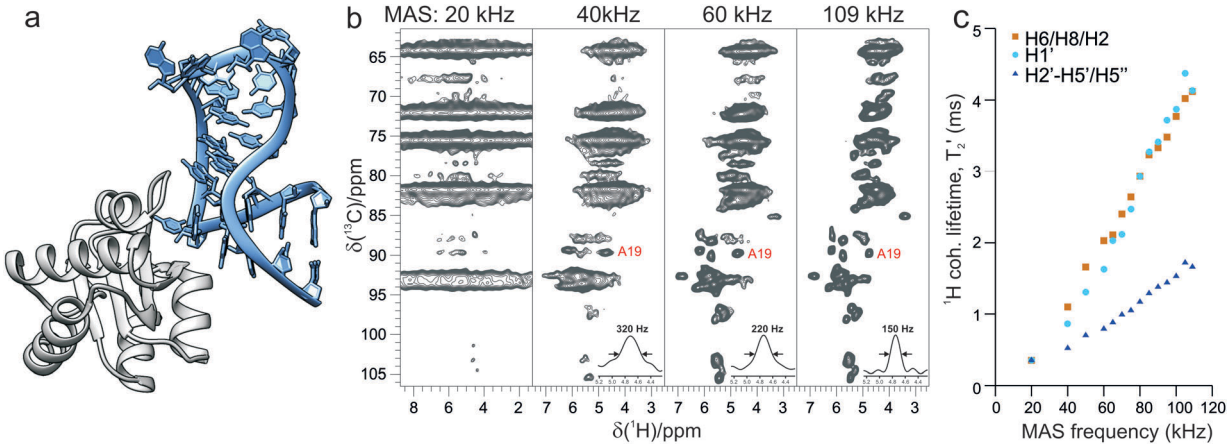

Fig. 1 (a) Structural model of the 26mer Box C/D RNA (light blue) bound to the L7Ae protein (grey) from *Pf*, established by alignment of the previously determined MAS NMR structure (PDB 2N0R)[3] of the RNA from *Pf* with a homologous RNA sequence in a larger complex (PDB 3NMU). (b) Ribose and base C5–H5 regions of ^{13}C–^{1}H CP-HSQC spectra recorded on a 800 MHz spectrometer at MAS rates of 20, 40, 60 and 109 kHz, characteristic for commercial 3.2, 1.9, 1.3 and 0.7 mm MAS probes. 1D traces of a representative resonance with the corresponding proton line width are shown in the bottom right corner. (c) Bulk coherence lifetimes (T_2') of base H6, H8 and H2 (brown squares), ribose H1′ (cyan circles) and other ribose H2′–H5″ protons (blue triangles) measured on a 800 MHz spectrometer and MAS frequencies from 20 to 109 kHz.

the identification of ^{1}H, ^{15}N and ^{13}C resonances of nucleotide spin-systems in the 26mer Box C/D RNA from a single, uniformly ^{13}C,^{15}N-labelled sample.

Fig. 1 shows the remarkable effect on ^{1}H resolution and sensitivity observed for the Box C/D RNA upon increase of the magic-angle spinning rates. 2D dipolar-based ^{13}C–^{1}H cross-polarization (CP)-HSQC experiments,[13] tailored for ribose resonances on a 800 MHz spectrometer, improve from a featureless spectrum at 20 kHz to a resolved fingerprint at 110 kHz MAS. ^{1}H line widths decrease substantially due to effective averaging of dipolar ^{1}H–^{1}H interactions, which is reflected by a nearly linear increase of the ^{1}H coherence lifetime (T_2') with MAS rates up to 110 kHz (Fig. 1c). In this forefront spinning regime, anomeric ribose H1′ and base H6/H8/H2 resonances reach above 4 ms of bulk T_2'; this corresponds to an 80 Hz homogeneous contribution to the ^{1}H line width of 130–170 Hz. At comparable MAS conditions, such long coherence lifetimes have been reported only for proteins in microcrystalline preparations featuring low dynamics.[14] The resolution of ribose H2′–H5′/H5″ resonances is lower, as these protons are involved in a stronger network of dipolar couplings; however, they feature better chemical shift dispersion than their carbon counterparts.[15,16] Seven C5–H5 correlations are visible out of the nine pyrimidines (Fig. S1a, ESI†).

Fig. 2 shows a magnification of the two anomeric and base ^{13}C–^{1}H fingerprints recorded on a 1 GHz spectrometer. Analogously to solution NMR, non-helical regions (δ(C1′) < 90 ppm, Fig. 2b) display the best dispersion of C1′–H1′ resonances. 2D ^{13}C–^{1}H correlations of base resonances are more overlapped (Fig. 2c), with only two bases showing distinct ^{13}C chemical shifts and line widths of 150 Hz (^{1}H) and 120 Hz (^{13}C). In the C2–H2 region (Fig. S1b, ESI†), five resonances can be resolved out of the nine As. The crowded appearance of the spectrum indicates a broader line width of most H8/H6 (purine/pyrimidine) with respect to the ribose ^{1}Hs. We hypothesized

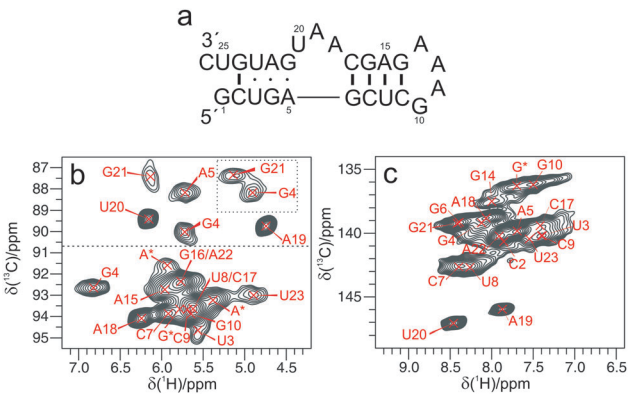

Fig. 2 (a) Sequence of the *Pf* 26mer Box C/D RNA. (b and c) Expansions of the ribose C1′–H1′ and base C6/8–H6/8 regions of ^{13}C–^{1}H CP-HSQC spectra recorded on a 1 GHz spectrometer and 111 kHz MAS. In (b) two resonances in the dotted box correspond to C4′–H4′ correlations, and the horizontal dashed line at approx. 90 ppm ^{13}C separates C1′–H1′ resonances of nucleotides located in helical and non-helical regions. The signals are labeled according to the ^{1}H assignment determined in this work and the previously reported sequence specific ^{13}C,^{15}N assignment.[2] The asterisk indicates resonances of non-assigned nucleotides.

that the broadening of the base resonances could stem from incomplete suppression of the dipolar interactions with either (i) the hydrogens of water molecules entering the major groove[17] or (ii) the close-by H2′s in helical regions. To test these two hypotheses we acquired CP-HSQC spectra on two additional samples: (i) L7Ae-Box C/D RNA complex dissolved in 90%/10% D_2O/H_2O rather than 100% H_2O. For this sample the H6/H8 line widths should not suffer from the vicinity to ^{1}Hs of the bound water; (ii) the L7Ae-Box C/D RNA complex with ^{2}H,^{12}C,^{14}N-C,U,A and ^{1}H,^{13}C,^{15}N-G, dissolved in 90%/10% D_2O/H_2O. For this sample the H8 line width of the ^{13}C,^{15}N-Gs should not suffer from the vicinity with the H2′s of the preceding nucleotides. The fingerprint in the base region is

almost identical for all samples (Fig. S1, ESI†), with a slight improvement of the line width in deuterated buffer. Thus, we conclude that the largest contribution to line broadening must be due to local structural heterogeneity that mostly affects the aromatic ^{1}H shifts.

In the following, we demonstrate that, despite the limited chemical shift dispersion of RNA, 14 spin systems can be established out of 19 nucleotides in the structured regions of the 26mer Box C/D RNA (excluding the loop and the ends) without resorting to nucleotide-specific labeling. This is possible due to efficient magnetization transfers at MAS >100 kHz and high-dimensional experiments.

Leveraging the high-sensitivity of the 2D (H)CH spectrum, we implemented an (H)NCH experiment. This is comparable to the (H)NCAHA experiment for proteins,[13,18] which we adapted to the topology of ^{1}H, ^{13}C and ^{15}N spins in RNA and to the distribution of ^{13}C chemical shifts. The experiment starts with a long-range ^{1}H–^{15}N transfer, followed by a band specific CP step tuned to either ribose or aromatic ^{13}C offsets, and yields either ribose-specific N1/N9–C1′–H1′ or base-specific N1–C6–H6/N9–C8–H8 correlations (Fig. 3a and b). The ^{15}N chemical shifts allow distinguishing pyrimidine from purine correlations (Fig. 3c and d) as well as associating C1′–H1′ with C6–H6/C8–H8 resonances. These correlations are similar to those established in solution NMR, with the advantage that the dipolar-based long-range ^{1}H–^{15}N and the one-bond ^{15}N–^{13}C transfers used here maintain high efficiencies even for large RNAs, due to the sufficiently long $T_{1\rho}$ relaxation times at fast MAS (>12 and 50 ms for ribose ^{1}H and ^{13}C, respectively; Fig. S3, ESI†). The ribose-specific (H)NCH spectrum shows excellent sensitivity (Fig. 3e–g); in less than 12 hours, resonances could be correlated for 17 out of the 19 previously assigned[2] spin systems (10 N9–C1′–H1′ and 7 N1–C1′–H1′ spin sets belonging to the region 3–10 and 15–23, with only nucleotides G14 and G24 missing, Table S4, ESI†). In the base-specific (H)NCH spectrum, the sensitivity of the transfer is affected by the multiple competitive coherence transfer pathways from the N1/N9 spins towards C2/C4 and C6/C8, as previously observed in CNC transfer schemes.[2] Nonetheless, we obtained correlations for 19 nucleotides in 26 hours.

At fast MAS rates, the long ^{13}C $T_{1\rho}$ relaxation times enable efficient scalar transfers between bonded ^{13}C atoms. These transfers allow establishing entire ribose spin systems in an efficient manner, as scalar ^{13}C transfers are easier to interpret than those based on proton-driven spin diffusion (PDSD) at slower MAS rates.[19] Scalar transfers can be triggered by inserting into the (H)CH module a rotor-synchronized, low-power TOBSY mixing,[20,21] or even less power-demanding schemes, such as WALTZ-16.[22] In the resulting HCCH-TOCSY[18,23] experiment, long mixing times (25 ms) are used to spread magnetization to all ribose ^{13}C spins. The information content can be maximized if both ^{1}H and ^{13}C shifts of starting and ending CH groups on

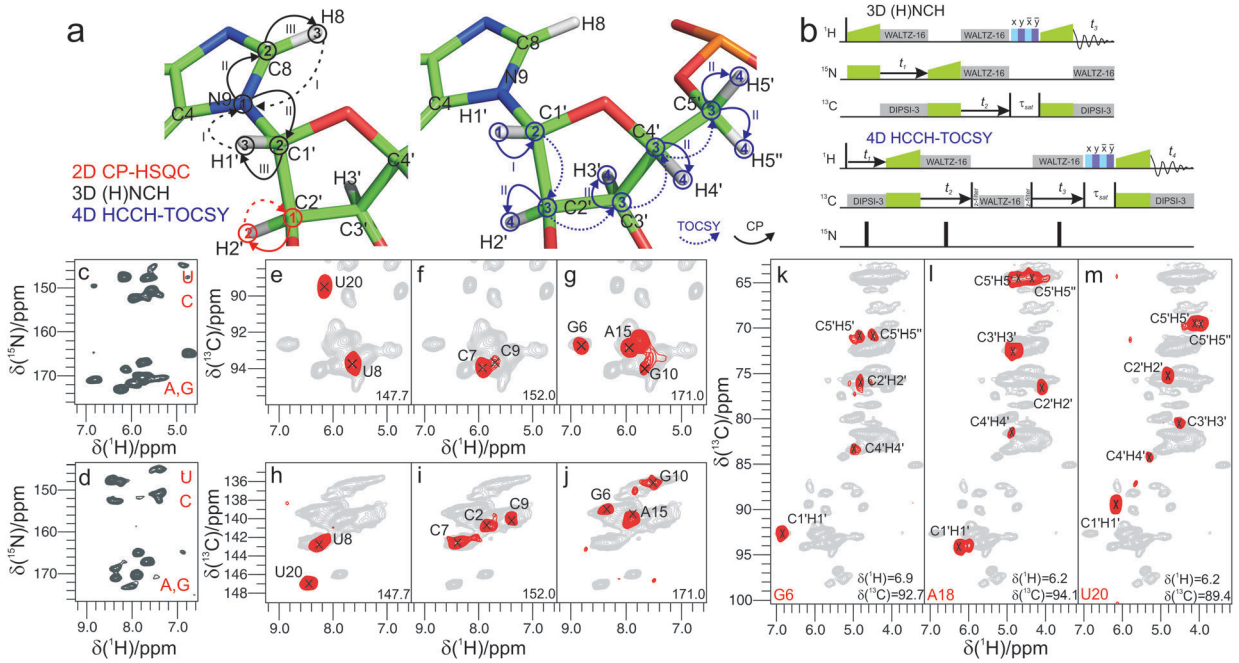

Fig. 3 (a and b) Magnetization transfer and radiofrequency irradiation schemes: 2D ^{13}C–^{1}H CP-HSQC (color-coded in red), 3D (H)NCH (in black), and 4D HCCH-TOCSY (in blue). Arabic numbers in (a) indicate spectral dimensions (t_1–t_4) in the pulse schemes (b); roman numbers indicate the CP transfers. (c and d) 2D ^{15}N(t_1)–^{1}H projections of 3D (H)NCH experiments tuned to either ribose or base resonances. (e–j) Representative ^{13}C–^{1}H cross-sections from the (H)NCH spectra showing either ribose N1/N9–C1′–H1′ (e–g) or base N1–C6–H6 or N9–C8–H8 correlations (h–j), at the ^{15}N frequency indicated in each panel. (k–m) Assignment of ribose spin systems with the 4D HCCH-TOCSY experiment. Representative 2D planes from the 4D experiment showing the spin systems of G6 (k), A18 (l), U20 (m). ^{1}H and ^{13}C frequencies are indicated in each panel. For reference, in panels (e–m) the red contours of either (H)NCH or HCCH-TOCSY spectra are overlaid onto 2D CP-HSQC spectra (in grey). (H)NCH spectra were recorded on a 1 GHz spectrometer at 111 kHz MAS, while the HCCH-TOCSY spectrum was recorded on a 800 MHz spectrometer at MAS frequency of 100 kHz.

the mixing pathway are recorded in a 4D dataset, using non-uniform sampling (NUS) to ensure spectral resolution.[24–28] 2D cross-sections from a 4D HCCH-TOCSY acquired for 3 days with exponentially relaxation-weighted random NUS,[29,30] are shown in Fig. 3k–m. For most residues, the separation of the H1′ and C1′ resonances translates into fully resolved planes displaying the entire ribose spin systems. For few nucleotides in helical regions (U8/G10/C17), low dispersion of the C1′ and H1′ chemical shifts prevents the separation of their spin systems. To lift this ambiguity, we designed a 4D (H)NCCH-TOCSY experiment, which uses the N1/N9 dimension to further separate overlapped ribose spin systems (Fig. S4, ESI†). Even with moderate sampling of the ^{15}N dimension, the experiment, which ran for 4.5 days, allows easy separation of purines and pyrimidines, as well as of spin systems within each subclass (U8 and C17, Fig. S4c–e, ESI†). All in all, we could unambiguously assign 14 out of 19 ribose spin systems in the structured part of the Box C/D RNA (Table S4, ESI†). The cross peak intensity of a few nucleotides was either low (G10, Fig. S4d, ESI†), or weak beyond detection (C2, C9, G14, A15 and G24). These nucleotides are mostly located in the junction or ends of secondary structure elements, where increased internal motions impair transfer efficiency during the two long CP steps required in ^{15}N-resolved multidimensional spectra (Fig. S4a and b, ESI†).

In summary, we demonstrate that ^{1}H-detection at fast MAS rates can be applied to nucleic acids and allows the assignment of ^{1}H, ^{13}C and ^{15}N resonances in nucleotide spin systems with only 200 μg of uniformly ^{13}C,^{15}N labeled RNA. In comparison to ^{13}C-detected experiments, ^{1}H-detection bypasses the need of nucleotide-type selectively labeled samples, resulting in a fast and cost-efficient route to site-specific studies. The strategy we devised is similar to that used in solution NMR, but has the advantage of being applicable to large RNAs or RNA–protein complexes. We are currently developing this strategy towards the sequential assignment of RNA resonances and the collection of structural restraints based on ^{1}H-detection. The RNA–protein complex used in this study was in microcrystalline form. However, all building blocks of the pulse sequences have been shown to perform also on non-crystalline formulations.[18,31–33] Given the difficulty of obtaining good-diffracting crystals for large RNA–protein complexes, we anticipate that these results will strengthen the role of MAS NMR in RNA structural biology, and more generally provide momentum in the atomic-level description of structure and dynamics of RNA.

TC was supported by the DFG (CA 294/10-1), GP by the ERC (ERC-2015-CoG GA 648974), and JS by a Marie Skłodowska-Curie fellowship (GA 661799 COMPLEX-FAST-MAS). The work was co-funded by Instruct, a part of the ESFRI, and supported by national member subscriptions, by CNRS (IR-RMN FR3050) and by the EU-project iNext (GA 653706).

Conflicts of interest

There are no conflicts to declare.

Notes and references

1 Y. C. Su, L. Andreas and R. G. Griffin, *Annu. Rev. Biochem.*, 2015, **84**, 465–497.
2 A. Marchanka, B. Simon and T. Carlomagno, *Angew. Chem., Int. Ed.*, 2013, **52**, 9996–10001.
3 A. Marchanka, B. Simon, G. Althoff-Ospelt and T. Carlomagno, *Nat. Commun.*, 2015, **6**, 7024.
4 V. Chevelkov, K. Rehbein, A. Diehl and B. Reif, *Angew. Chem., Int. Ed.*, 2006, **45**, 3878–3881.
5 Ü. Akbey, S. Lange, W. T. Franks, R. Linser, K. Rehbein, A. Diehl, B. J. van Rossum, B. Reif and H. Oschkinat, *J. Biomol. NMR*, 2010, **46**, 67–73.
6 S. Asami, M. Rakwalska-Bange, T. Carlomagno and B. Reif, *Angew. Chem., Int. Ed.*, 2013, **52**, 2345–2349.
7 J. R. Lewandowski, J. N. Dumez, Ü. Akbey, S. Lange, L. Emsley and H. Oschkinat, *J. Phys. Chem. Lett.*, 2011, **2**, 2205–2211.
8 A. J. Nieuwkoop, W. T. Franks, K. Rehbein, A. Diehl, Ü. Akbey, F. Engelke, L. Emsley, G. Pintacuda and H. Oschkinat, *J. Biomol. NMR*, 2015, **61**, 161–171.
9 Y. Yang, S. Xiang, X. Liu, X. Pei, P. Wu, Q. Gong, N. Li, M. Baldus and S. Wang, *Chem. Commun.*, 2017, **53**, 12886–12889.
10 L. B. Andreas, T. Le Marchand, K. Jaudzems and G. Pintacuda, *J. Magn. Reson.*, 2015, **253**, 36–49.
11 A. Böckmann, M. Ernst and B. H. Meier, *J. Magn. Reson.*, 2015, **253**, 71–79.
12 T. Schubeis, T. Le Marchand, L. B. Andreas and G. Pintacuda, *J. Magn. Reson.*, 2018, **287**, 140–152.
13 D. H. Zhou, G. Shah, M. Cormos, C. Mullen, D. Sandoz and C. M. Rienstra, *J. Am. Chem. Soc.*, 2007, **129**, 11791–11801.
14 L. B. Andreas, K. Jaudzems, J. Stanek, D. Lalli, A. Bertarello, T. Le Marchand, D. C. D. Paëpe, S. Kotelovica, I. Akopjana, B. Knott, S. Wegner, F. Engelke, A. Lesage, L. Emsley, K. Tars, T. Herrmann and G. Pintacuda, *Proc. Natl. Acad. Sci. U. S. A.*, 2016, **113**, 9187–9192.
15 B. Fürtig, C. Richter, J. Wöhnert and H. Schwalbe, *ChemBioChem*, 2003, **4**, 936–962.
16 A. Marchanka and T. Carlomagno, *eMagRes*, 2014, **3**, 119–128.
17 M. Egli, S. Portmann and N. Usman, *Biochemistry*, 1996, **35**, 8489–8494.
18 J. Stanek, L. B. Andreas, K. Jaudzems, D. Cala, D. Lalli, A. Bertarello, T. Schubeis, I. Akopjana, S. Kotelovica, K. Tars, A. Pica, S. Leone, D. Picone, Z. Q. Xu, N. E. Dixon, D. Martinez, M. Berbon, N. El Mammeri, A. Noubhani, S. Saupe, B. Habenstein, A. Loquet and G. Pintacuda, *Angew. Chem., Int. Ed.*, 2016, **55**, 15503–15509.
19 V. Agarwal, S. Penzel, K. Szekely, R. Cadalbert, E. Testori, A. Oss, J. Past, A. Samoson, M. Ernst, A. Böckmann and B. H. Meier, *Angew. Chem., Int. Ed.*, 2014, **53**, 12253–12256.
20 E. H. Hardy, R. Verel and B. H. Meier, *J. Magn. Reson.*, 2001, **148**, 459–464.
21 K. O. Tan, V. Agarwal, N. A. Lakomek, S. Penzel, B. H. Meier and M. Ernst, *Solid State Nucl. Magn. Reson.*, 2018, **89**, 27–34.
22 A. J. Shaka, J. Keeler, T. Frenkiel and R. Freeman, *J. Magn. Reson.*, 1983, **52**, 335–338.
23 A. Bax, G. M. Clore and A. M. Gronenborn, *J. Magn. Reson.*, 1990, **88**, 425–431.
24 M. Huber, S. Hiller, P. Schanda, M. Ernst, A. Böckmann, R. Verel and B. H. Meier, *ChemPhysChem*, 2011, **12**, 915–918.
25 S. Xiang, V. Chevelkov, S. Becker and A. Lange, *J. Biomol. NMR*, 2014, **60**, 85–90.
26 R. Linser, B. Bardiaux, L. B. Andreas, S. G. Hyberts, V. K. Morris, G. Pintacuda, M. Sunde, A. H. Kwan and G. Wagner, *J. Am. Chem. Soc.*, 2014, **136**, 11002–11010.
27 S. Paramasivam, C. L. Suiter, G. Hou, S. Sun, M. Palmer, J. C. Hoch, D. Rovnyak and T. Polenova, *J. Phys. Chem. B*, 2012, **116**, 7416–7427.
28 I. V. Sergeyev, B. Itin, R. Rogawski, L. A. Day and A. E. McDermott, *Proc. Natl. Acad. Sci. U. S. A.*, 2017, **114**, 5171–5176.
29 J. C. J. Barna, E. D. Laue, M. R. Mayger, J. Skilling and S. J. P. Worrall, *J. Magn. Reson.*, 1987, **73**, 69–77.
30 D. Rovnyak, J. C. Hoch, A. S. Stern and G. Wagner, *J. Biomol. NMR*, 2004, **30**, 1–10.
31 J. M. Lamley, D. Iuga, C. Oster, H. J. Sass, M. Rogowski, A. Oss, J. Past, A. Reinhold, S. Grzesiek, A. Samoson and J. R. Lewandowski, *J. Am. Chem. Soc.*, 2014, **136**, 16800–16806.
32 P. Schanda, S. Triboulet, C. Laguri, C. M. Bougault, I. Ayala, M. Callon, M. Arthur and J. P. Simorre, *J. Am. Chem. Soc.*, 2014, **136**, 17852–17860.
33 H. R. W. Dannatt, M. Felletti, S. Jehle, Y. Wang, L. Emsley, N. E. Dixon, A. Lesage and G. Pintacuda, *Angew. Chem., Int. Ed.*, 2016, **55**, 6638–6641.